

Restoration of User Videos Shared on Social Media

Hongming Luo

College of Electronics and Information Engineering,
Shenzhen University, China
luohongming2018@email.szu.edu.cn

Kin-Man Lam

Department of Electronic and Information Engineering,
The Hong Kong Polytechnic University, China
enklam@polyu.edu.hk

Fei Zhou*

College of Electronics and Information Engineering,
Shenzhen University, China
flying.zhou@163.com

Guoping Qiu^{†‡}

College of Electronics and Information Engineering,
Shenzhen University, China
qiu@szu.edu.cn

ABSTRACT

User videos shared on social media platforms usually suffer from degradations caused by unknown proprietary processing procedures, which means that their visual quality is poorer than that of the originals. This paper presents a new general video restoration framework for the restoration of user videos shared on social media platforms. In contrast to most deep learning-based video restoration methods that perform end-to-end mapping, where feature extraction is mostly treated as a *black box*, in the sense that what role a feature plays is often unknown, our new method, termed Video restOration through adapTive dEgradation Sensing (VOTES), introduces the concept of a degradation feature map (DFM) to explicitly guide the video restoration process. Specifically, for each video frame, we first adaptively estimate its DFM to extract features representing the difficulty of restoring its different regions. We then feed the DFM to a convolutional neural network (CNN) to compute hierarchical degradation features to modulate an end-to-end video restoration backbone network, such that more attention is paid explicitly to potentially more difficult to restore areas, which in turn leads to enhanced restoration performance. We will explain the design rationale of the VOTES framework and present extensive experimental results to show that the new VOTES method outperforms various state-of-the-art techniques both quantitatively and qualitatively. In addition, we contribute a large scale real-world database of user videos shared on different social media platforms. Codes and datasets are available at <https://github.com/luohongming/VOTES.git>

*Also with [1]Peng Cheng Laboratory, Shenzhen [2]Guangdong Key Laboratory of Intelligent Information Processing, Shenzhen, China.

[†]The corresponding author.

[‡]Also with [1]Shenzhen Key Laboratory of Digital Creative Technology, [2]Shenzhen Institute for Artificial Intelligence and Robotics for Society [3]Guangdong-Hong Kong Joint Laboratory for Big Data Imaging and Communication, China.

Permission to make digital or hard copies of all or part of this work for personal or classroom use is granted without fee provided that copies are not made or distributed for profit or commercial advantage and that copies bear this notice and the full citation on the first page. Copyrights for components of this work owned by others than ACM must be honored. Abstracting with credit is permitted. To copy otherwise, or republish, to post on servers or to redistribute to lists, requires prior specific permission and/or a fee. Request permissions from [permissions@acm.org](https://permissions.acm.org).

MM '22, October 10–14, 2022, Lisbon, Portugal.

© 2022 Association for Computing Machinery.

ACM ISBN 978-1-4503-9203-7/22/10...\$15.00

<https://doi.org/10.1145/3503161.3547847>

CCS CONCEPTS

• Computing methodologies → Image processing.

KEYWORDS

social media, video restoration, degradation sensing

ACM Reference Format:

Hongming Luo, Fei Zhou, Kin-Man Lam, and Guoping Qiu. 2022. Restoration of User Videos Shared on Social Media. In *Proceedings of the 30th ACM International Conference on Multimedia (MM '22)*, October 10–14, 2022, Lisbon, Portugal. ACM, New York, NY, USA, 9 pages. <https://doi.org/10.1145/3503161.3547847>

1 INTRODUCTION

The number of videos shared on social media platforms is experiencing explosive growth and hundreds of thousands of hours of videos are uploaded by hundreds of millions of users every day. Unknown to most social media users, videos directly shared with friends, such as on WeChat or uploaded to a server, such as on YouTube, are processed by the social media platforms to save transmission bandwidth and storage space. Even though different platforms use unknown proprietary technologies, through inspecting the source videos and the versions visible to the viewers, we discover that the transmitted videos on all platforms will have two general types of degradation, resolution reduction and noisy content. As a result, all videos shared on social media invariably have poorer quality, compared to the originals. Although, in most cases, the social media versions are of good enough quality, they nevertheless have suffered quality degradation which, in many cases, may affect viewing experience.

In this paper, we aim to restore user videos shared on social media. Generally speaking, this process involves two widely researched areas, video spatial resolution enhancement (super-resolution) [29] [31] [24] [1] and video restoration for recovering information lost during compression and other processing [20] [27] [30] [5]. Although video super-resolution and restoration have been popular research topics for many years, these quality issues in user videos shared on social media platforms seem to have not been recognised and addressed before. This paper makes the following contributions:

(1) We present a new general video restoration framework. In contrast to most deep learning-based video restoration methods that perform end-to-end mapping where feature extraction is mostly treated as a *black box*, in the sense that what role a feature plays

is unknown and indeed, if a feature is useful or necessary is often very difficult to determine, our new method, termed Video restoration through adaptive dEgradation Sensing (VOTES), introduces the concept of a degradation feature map (DFM) to guide the video restoration process. Specifically, for each video frame, we first adaptively estimate its DFM to extract features representing the difficulty of restoring specific regions. We then feed the DFM to a CNN to compute hierarchical degradation features to modulate an end-to-end video restoration network, such that more attention is paid explicitly to potentially more difficult to restore areas, which in turn leads to enhanced restoration performance.

(2) We present a large scale real-world database of user videos shared on social media (UVSSM) for the purposes of researching the problem of restoring videos degraded by unknown processes and procedures in general, and for developing practical solutions to the restoration of user videos shared on different social media platforms in particular. The UVSSM database contains over 350 pairs of original and shared videos obtained from four popular social media platforms including Bilibili, Twitter, WeChat and YouTube.

We will explain the design rationale of the VOTES framework and present extensive experimental results to show that the new VOTES method outperforms various state-of-the-art video restoration techniques both quantitatively and qualitatively.

2 RELATED WORK

Various CNN-based techniques have been developed for video restoration, which can be divided into two categories: single-frame restoration and multiple-frame restoration. For single-frame restoration, most methods concentrate on designing various architectures to achieve end-to-end restoration. They rely on the capacity of advanced CNN architectures to learn from training samples. Some architectures are based on diverse skip-connection techniques, such as VDSR[10], EDSR[14], and RDN[31]. Attention mechanisms are also introduced to exploit the capability of CNN, like RCAN[29], SAN[3], and NLSN[15]. Using an end-to-end training strategy, many architectures are capable of tackling different restoration problems, such as super-resolution, compression artifact reduction, and denoising [27][30]. In multiple-frame restoration methods, more focus is on exploiting the relative information from neighboring frames. A number of methods, such as [1] for super-resolution and [7] for compressed video enhancement, utilize optical flow between multiple frames to aggregate information. Deformable convolution networks[32] have been successfully applied to video restoration, e.g., EDVR[24] and TDAN[21]. Recurrent network structures have also been used, such as FRVSR [17] and RSDN [8]. However, these methods only deal with the problem of a single degradation, e.g., down-scaling or compression, while real-world videos may suffer from multiple types of degradation.

Recognizing the drawbacks of the above methods, researchers have developed methods to process videos with multiple types of degradation. Zhang, *et al.* [28] proposed a single model to perform SR and denoising jointly, while [26] used USRNet to handle degradation caused by scaling, blurring, and noise. SFTMD[6] introduced a prediction network and a corrector network to better estimate the degradation parameters. Furthermore, Wang, *et al.* [23] suggested

that the degradation parameters should be learned from the input image.

There exist very few works that simultaneously tackle compression artifact reduction and resolution enhancement. The CISRD-CNN model [2] consists of three cascaded modules to enhance resolution and reduce compression artifacts simultaneously. The COMISR model [13] focuses on compressed video SR, where a bi-directional recurrent module and a Laplacian enhancement module were proposed to improve the performance. As social media videos may have been subjected to various processing, local areas may have different degrees of degradation, we will make use of a pixel-wise degradation measurement to develop a novel degradation-sensing-based video restoration method.

3 PROPOSED METHOD

3.1 Overview

Through sharing videos on several social media platforms, such as WeChat, YouTube, Bilibili, and Twitter, we discover that all videos that are viewable on these platforms have poorer quality than their originals. Clearly, various kinds of degradation have occurred. With reference to Figure 1, the original video $y = \{\dots, y_{t-1}, y_t, y_{t+1}, \dots\}$, where y_t is the frame at time instance t , y is degraded by unknown operators of the social media platforms to produce a version of the video $x = \{\dots, x_{t-1}, x_t, x_{t+1}, \dots\}$, to be shared. Comparing the shared and the original videos, there are two notable characteristics. Firstly, there is often aliasing caused by spatial sub-sampling, for example, WeChat will down-scale the videos to a fixed resolution of 960×540 or 1280×720 . However, specific sub-sampling algorithms used are unknown. Secondly, the shared videos often contain various artifacts and missing details, and clearly, compression has been applied. Again, specific algorithms used are also unknown. Therefore, we are facing with the problem of restoring videos that have gone through unknown degradation procedures.

In most deep learning-based video restoration models, e.g., [24][7][9], x will be used as input to a CNN architecture to recover y in an end-to-end manner. Different methods differ mainly in the designs of the CNN architecture and how the frames are handled. As a characteristic of CNN/deep learning-based solutions, these methods all involve various feature extraction techniques. However, a common problem with these methods is the "black box" phenomenon, where the role a feature plays is unknown and indeed, it is often very difficult to determine if a feature is useful or necessary.

In contrast, we aim to extract meaningful features that can serve specific purposes for solving the problem we are facing. From observing degraded videos, it is easy to find that the degree of degradation varies in different clips of a video and in different regions of a frame. For example, as shown in Figure 2 (a) and (b), the degradation in the flat regions is not noticeable, while that in the texture or edge regions is apparent. Obviously, the restoration of the heavily degraded regions is more difficult, therefore, these regions need more attention paid to them. If, for each frame, we can obtain a pixel-wise map to estimate the degradation each location has suffered, then we can use this map to guide the design of the restoration model to enhance performance.

Based on the above discussion, we propose the Video restoration through adaptive dEgradation Sensing (VOTES) framework

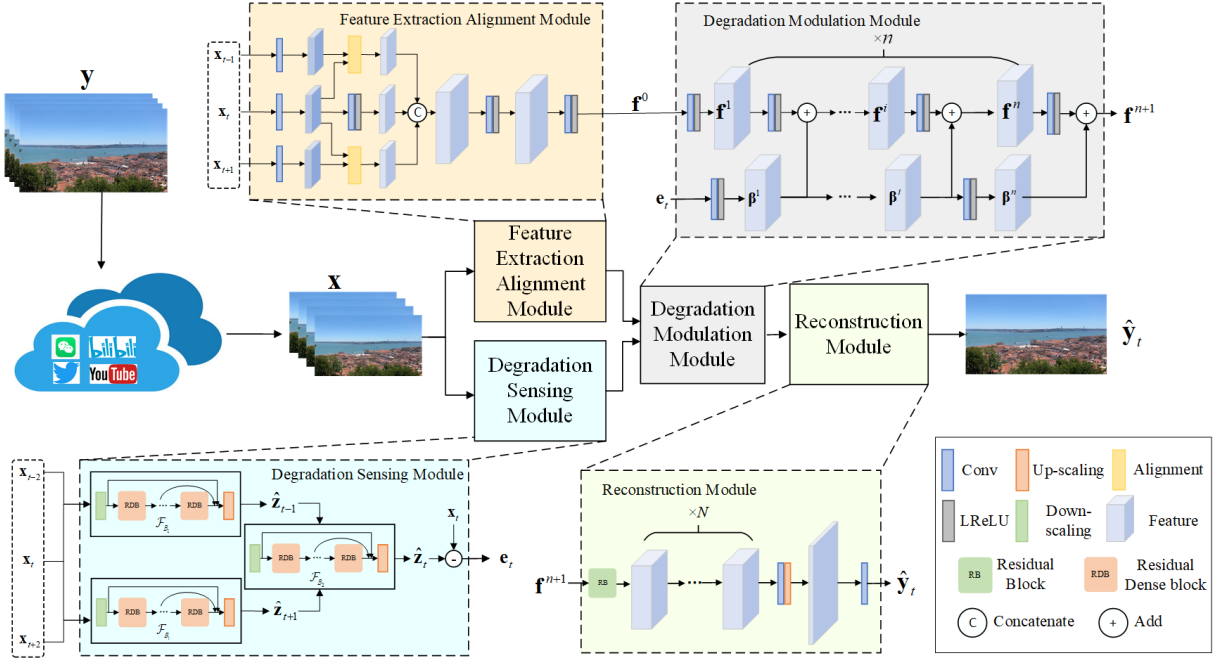


Figure 1: Overall framework of the Video restORation through adapTive dEGradation Sensing (VOTES) model. The original video y is degraded by social media platforms to x . VOTES first tries to estimate a degradation feature map (DFM) e using the degradation sensing module (DSM). Convolutional blocks are used to process e to extract features. To restore x , multiple frames of x are first passed through a feature extraction and alignment module (FEAM) to extract frame aligned features, which are then passed to the degradation modulation module (DMM). Finally the features are fed to the reconstruction module before outputting a restored video \hat{y} . The FEAM and DSM architectures in this figure are simplified for illustration purpose. For implementation details, please refer to Section 5.1.

as shown in Figure 1. Before directly restoring the input video x , a degradation sensing module (details to be described later) is proposed to extract a degradation feature map (DFM) e adaptively from the input video x . The DFM e contains degradation information, indicating which locations have suffered more degradation and therefore, would be more difficult to recover, and that any restoration models should pay particular attention to such regions. With DFM, we introduce the degradation modulation module (DMM) as a plug-in module to the end-to-end video restoration model to guide it to somehow pay more attention to areas that have suffered heavier degradation.

3.2 Degradation Sensing Module

The degradation sensing module aims to estimate the DFM from the input video x . For any given x , we can always assume there is a higher quality reference video z , from which x is derived, where x and z have the same spatial resolution. If we can estimate z , then the DFM e can be obtained:

$$e = \hat{z} - x, \quad (1)$$

where \hat{z} is an estimated version of z . In order to obtain \hat{z} , we design the degradation sensing module as shown in Figure 1 through learning. Specifically, a learning module \mathcal{F}_{B_1} is designed to first estimate \hat{z}_{t-1} and \hat{z}_{t+1} from three frames $\{x_{t-2}, x_t, x_{t+2}\}$. Then, we design another learning module \mathcal{F}_{B_2} to estimate \hat{z}_t . The process of

estimating z can be summarised as follows:

$$\hat{z}_{t-1} = \mathcal{F}_{B_1}(x_{t-2}, x_t), \quad (2)$$

$$\hat{z}_{t+1} = \mathcal{F}_{B_1}(x_{t+2}, x_t), \quad (3)$$

$$\hat{z}_t = \mathcal{F}_{B_2}(\hat{z}_{t-1}, \hat{z}_{t+1}). \quad (4)$$

There is considerable flexibility in designing \mathcal{F}_{B_1} and \mathcal{F}_{B_2} . The implementation specifics used in this paper are described in Section 5.1. Once we obtain \hat{z} , the DFM e can be calculated according to (1). In order to suppress excessively large values as well as to highlight small values, we process the DFM by a logarithmic function, as in (5).

$$e = \frac{1}{S} \log(|\hat{z} - x| + 1), \quad (5)$$

where $S = \max(\log(|\hat{z} - x| + 1))$, and the bias 1 is used to guarantee all pixels in the DFM are positive. We will use the DFM in (5) to guide the design of an end-to-end video restoration model. Figure 2 (c) and (d) illustrate an example of such a map and its relation to the restoration errors by one of the state-of-the-art methods [24]. It is seen that when an area in the DFM has a smaller value, the algorithm can better restore that area resulting in a smaller error. On the other hand, when an area in the DFM has a larger value, the algorithm will have more difficulty in recovering the missing details resulting in a larger error. More examples will be shown in Section 5.4.

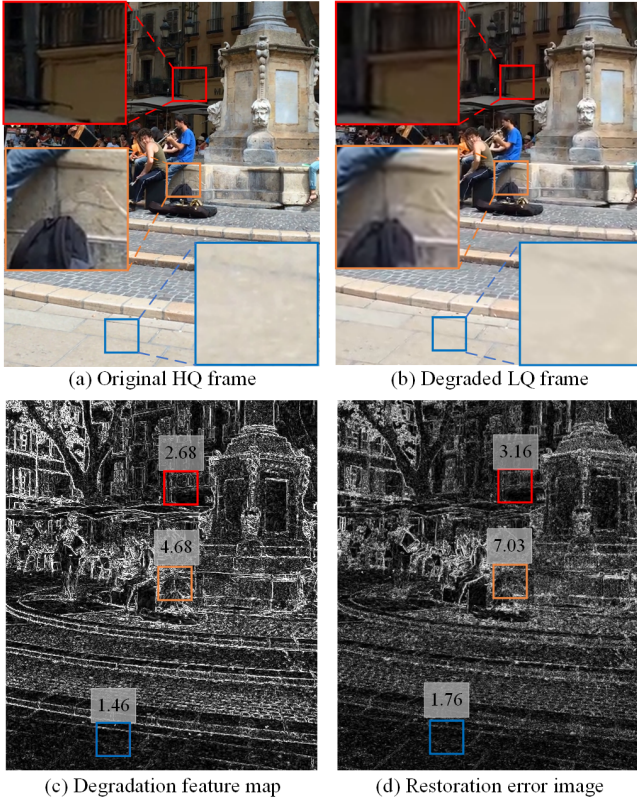


Figure 2: (a) An original high-quality frame and 3 enlarged patches. (b) Corresponding degraded low-quality frame. (c) The DFM of the degraded frame. (d) Restoration error by a state-of-the-art method [24]. The numbers above the squares are the average element values in the corresponding squares. Note the original resolution of (c) is half of that of (d), it is resized here for visualization convenience.

3.3 End-to-End Video Restoration through Adaptive Degradation Sensing

Many end-to-end video restoration models that use advanced CNN architectures have emerged, examples include 3D CNN [9], deformable convolutional network [24] and recurrent neural network [8]. A common design strategy in the literature is to take multiple frames of \mathbf{x} as input to a deep neural network model, which will normally contain a feature extraction and alignment module (FEAM), as shown in Figure 1, to extract representative features of the aligned frames. The output of the FEAM which is normally a multichannel feature map will then be processed by more convolutional blocks. Finally, the features are fed into the reconstruction module before outputting a restored frame.

Unlike those designs in the literature, the new VOTES solution is explicitly designed to restore videos with the help of the DFM. Specifically, we propose a degradation modulation module (DMM) as a plug-in to the end-to-end restoration model. DMM extracts hierarchical degradation features from the DFM to modulate the end-to-end restoration backbone network’s feature extractors. As shown in

Figure 1, the DFM \mathbf{e} is first fed into n cascaded convolutional blocks to extract hierarchical degradation features $\beta^1, \beta^2, \dots, \beta^n$ which are then used to modulate the feature maps of the end-to-end network as follows:

$$\mathbf{f}^{i+1} = LReLU(Conu(\mathbf{f}^i)) + \beta^i, \quad (6)$$

where $LReLU(\cdot)$ and $Conu(\cdot)$ are the non-linear activation with the negative slope set as 0.1 and the convolutional operation with kernel size of 3×3 . \mathbf{f}^i represents the modulated features after the i -th block, and \mathbf{f}^0 is the output of the FEAM and $\beta^0 = \mathbf{0}$. The modulated feature \mathbf{f}^{n+1} of the last block is passed into a reconstruction module, which contains a series of residual blocks. Finally, the output feature from the residual blocks is fed into two convolutional layers and an up-sampling layer to output the final result. With the help of the DFM and its hierarchical feature representations, the end-to-end network will be able to better extract features in areas that are more difficult to restore, thus achieving the aim of improving the performance of video restoration.



Figure 3: Some example scenes from the UVSSM dataset.

Table 1: Information about the UVSSM dataset.

| | WeChat | Twitter | Bilibili | YouTube |
|---------------|-----------|----------|----------|----------|
| Original res. | 1920x1080 | 1280x720 | 1280x720 | 1280x720 |
| Shared res. | 960x540 | 640x360 | 640x360 | 640x360 |
| No. of videos | 214 | 50 | 50 | 50 |

3.4 Model Training and Loss Functions

Model training is implemented in two stages. In the first stage, we need to estimate the reference video frames \mathbf{z}_t to recover $\hat{\mathbf{z}}$. Therefore we first train the networks \mathcal{F}_{B_1} and \mathcal{F}_{B_2} using the following loss function:

$$\mathcal{L}_{FI} = \sum_{j=t-1}^{t+1} |\hat{\mathbf{z}}_j - \mathbf{z}_j|, \quad (7)$$

where \mathbf{z}_j is down-scaled from the original frame \mathbf{y}_j which can be implemented using any image down-scaling technique, and in this paper we use the bicubic method. In the second stage, we train the rest of the system to optimize the following Charbonnier penalty function[12]:

$$\mathcal{L} = \sqrt{(\mathbf{y}_t - \hat{\mathbf{y}}_t)^2 + \epsilon^2}, \quad (8)$$

where $\epsilon = 10^{-3}$ as defined in [12].

4 USER VIDEOS SHARED ON SOCIAL MEDIA DATASET

To facilitate research into the restoration of user videos shared on social media, we have constructed a dataset, called user videos shared on social media (UVSSM). We first gathered 264 videos with lengths ranging from 5 to 30 seconds. These videos have a frame rate of 30 fps and come from two sources: mobile phone cameras and the Internet. The spatial resolutions of these original videos are either 1920×1080 or 1280×720 in high quality H.264 format. These videos contain a variety of content including people, animals, natural landscapes, city views, and many other objects and scenes. Figure 3 shows some example scenes from the dataset which will be made publicly available. All source videos in the UVSSM dataset have a Creative Commons Attribution licence (reuse allowed).

We then upload these original videos onto social media platforms. WeChat is a real-time instant transmission platform where any video sent to a friend will reach the destination almost immediately. Any video, regardless of its original resolution, will be scaled to 960×540 (if the original is smaller than this then it is unchanged). We have used five different brands of mobile phones to share 214 videos on WeChat. We mainly conduct video restoration experiments on the WeChat platform to compare the restoration performance. In addition, to analyse the generalization performance of VOTES, we also include three other platforms, Twitter, Bilibili, and YouTube. The videos are uploaded onto their servers and users can choose several different resolution options to play. To construct the dataset on these three platforms, we upload 50 videos that are not included in the 214 shared on WeChat to each of the three platforms. The original resolution of these 50 videos is 1280×720 and we download them to 640×360 . Therefore the UVSSM dataset contains a total of 364 pairs of original and shared videos (214 WeChat, 50 Bilibili, 50 Twitter and 50 YouTube). The details of these videos are shown in Table 1 and more details are shown in the supplementary material.

5 EXPERIMENTS

5.1 Implementation Details and Datasets

We first perform experiments using the videos shared on WeChat by randomly picking 10 videos as the testing set, four videos as the validation set and the remaining 200 videos as the training set. To better evaluate the proposed method, we implement k-fold cross-validation. We conduct the experiments five times based on the above data division rules and calculate the average results. We use the videos from the other three platforms to evaluate the generalization capability of models trained with videos shared on WeChat. In addition, we also evaluate our method on a widely used SR dataset, REDS, which contains high-quality videos from NTIRE19 Competition [16]. REDS consists of 240 training clips, 30 validation clips and 30 testing clips (each with 100 frames). As the REDS dataset is uncompressed, we generate low-quality videos by down-scaling and compressing the originals using the H.264[25] codec with different quality parameters QP (QP=28,33) and different scale factors ($\times 2$, $\times 4$) via the Ffmpeg [22] toolbox. Since the ground truth of the testing set is not available, we use the validation set as our testing set. The 240 clips in the training set are randomly divided into 236 training clips and four validation clips in the experiments.

The feature extraction and alignment module (FEAM) in Figure 1 can be implemented by any feature extraction and alignment techniques and we adopt the pyramid cascaded network of EDVR [24]. The reconstruction module consists of 40 residual blocks *i.e.*, $N = 40$ as in EDVR. Five consecutive frames are fed to the FEAM to obtain aligned features. Besides, the learnable network \mathcal{F}_{B_1} and \mathcal{F}_{B_2} in the degradation sensing module are implemented based on the backbone network in BIN [18]. We adopt 10 convolutional blocks in the degradation modulation module, *i.e.*, $n = 10$. The channel size in each convolutional blocks is set to 64 except for the one in the output layer, which is set to three. The up-sampling operator is a pixel shuffle operator, defined in [19]. More details about the network structure are shown in supplementary material. We use RGB patches of size 128×128 as targets and 64×64 or 32×32 as inputs. The mini-batch size is set to 32 and we augment the training data with random flips and 90° rotations. Our model is trained with Adam optimizer [11] by setting the two parameters as (0.9, 0.999). The learning rate is initialized as 2×10^{-4} . We train the first stage for 10^6 iterations and train the second stage for 5×10^6 iterations. We implement our models with the PyTorch framework and train them using 4 NVIDIA Tesla P40 GPUs.

5.2 Comparison with State-of-the-art Methods

There exist very few works in the literature that explicitly address the problem of degraded (compressed) video super-resolution. In order to compare the new method with state-of-the-art (SOTA) methods, we have implemented two-stage solutions where a SOTA compressed video restoration model is first used to restore the video and then a SOTA SR model is used to enhance the resolution of the restoration results. For video restoration, we use STDF [4] which is a recent SOTA method. For resolution enhancement, we have experimented with four recent methods, including EDVR [24], RSDN [8], VSRTGA [9], and BasicVSR [1]. In addition, a one-stage method, COMISR [13] is also included in the comparison. We carefully implemented these methods by running the publicly available codes and use the same training and testing sets as those in the construction of our models. The quantitative results on REDS and UVSSM are shown in Table 2. Notably, our model achieves PSNR improvements of around 1.5 dB against other models on UVSSM, and it also achieves the best performance on REDS for different scaling factors and different quality factors.

Qualitative results in Figure 4 and Figure 5 also demonstrate the superiority of the new VOTES model. From the visual comparisons, we can see that video frames recovered by the new VOTES technique have more restored details. More visual results can be found in supplementary material.

5.3 Generalization capability of VOTES

As shown in the first column of Figure 6, the distortions of the same video shared on different platforms are not the same. In order to evaluate the generalization capability of our model from one platform to another, we apply the model trained on WeChat videos to process videos shared on the other three platforms and only fine-tune the trained model. For each platform, the 50 videos are randomly split into 40 for training and 10 for testing. We fine-tune one model for each of the three platforms separately.

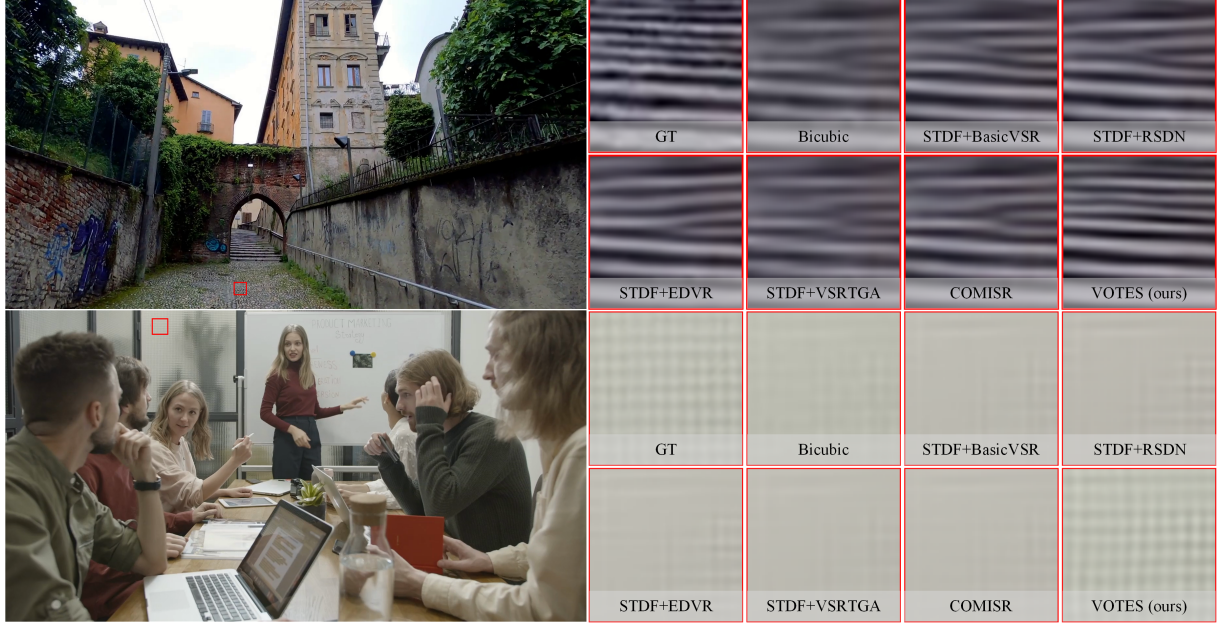


Figure 4: Qualitative comparison of video frames in UVSSM restored by different methods. The scaling factor is 2. Zoom-in for better visualization.

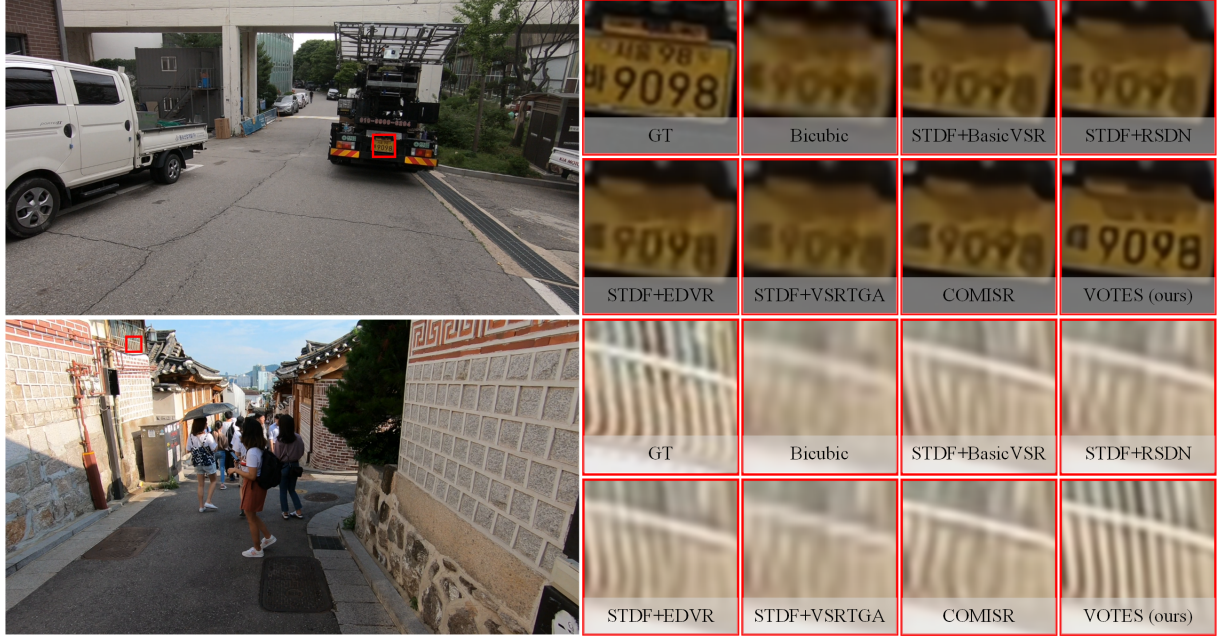


Figure 5: Qualitative comparison of video frames in REDS restored by different methods. The QP is 28 and scaling factor is 2. Zoom-in for better visualization.

The performance-improvement curves as fine-tuning epoch increases are shown in Figure 7, where "WeChat->Bilibili", "WeChat->Twitter" and "WeChat->YouTube" represent the model pre-trained on WeChat data and fine-tuned on Bilibili, Twitter and YouTube data, respectively. In addition to the cross-platforms experiments,

we also conduct cross-dataset experiments and apply the VOTES model, trained on UVSSM videos, to process the testing set of the low-quality videos in the REDS dataset. Results are also shown in Figure 7, where "UVSSM->REDS_QP28" represents the model pre-trained on UVSSM data and fine-tuned on the REDS training

Table 2: Quantitative comparison of performance on REDS and UVSSM (PSNR(dB)/SSIM). Due to UVSSM only contains $\times 2$ paired data, we only conduct $\times 2$ SR experiments on UVSSM. Blod text indicates the best.

| datasets | scale | QP | STDF[4]+RSDN[8] | STDF+EDVR[24] | STDF+VSRTGA[9] | STDF+BasicVSR[1] | COMISR[13] | VOTES(ours) |
|----------|------------|----|-----------------|---------------|----------------|------------------|--------------|---------------------|
| REDS | $\times 2$ | 28 | 31.4/0.8487 | 31.54/0.8511 | 30.29/0.8247 | 31.45/0.8494 | 31.11/0.8465 | 32.15/0.8644 |
| | | 33 | 29.55/0.7926 | 29.59/0.7934 | 29.01/0.7775 | 29.57/0.7930 | 29.39/0.7912 | 29.95/0.8043 |
| | $\times 4$ | 28 | 27.66/0.7287 | 27.79/0.7326 | 27.68/0.7291 | 27.8/0.7329 | 27.10/0.7170 | 28.08/0.7441 |
| | | 33 | 26.41/0.6842 | 26.44/0.6861 | 26.40/0.6841 | 26.47/0.6863 | 26.08/0.6777 | 26.61/0.6942 |
| UVSSM | $\times 2$ | - | 31.40/0.8781 | 31.67/0.8790 | 31.23/0.8681 | 31.59/0.8783 | 31.35/0.8755 | 33.01/0.8945 |

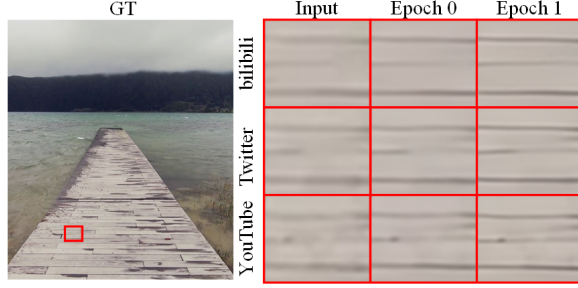


Figure 6: Illustration of the generalization capability of the VOTES model. Left: a video frame. Right: Enlarged patches of the red square on the left image. The 1st column shows the patch shared on different social media platforms. It is seen that different platforms process the video differently and introduce different degradation. The 2nd column shows the patch processed directly by the model trained on data from WeChat. It is seen that more details are visible demonstrating that the model has good generalization capability. The 3rd column shows the patch restored by the model after it has been fine-tuned for one epoch. It is seen that more details have been recovered.

data for the quality factor of 28. It is seen that only a few training epochs are required for the VOTES model to reach convergence. For the cross-platforms experiments, our model takes one epoch to achieve a performance that is only 0.1 dB below the best performance. An example of visual quality improvement is shown in Figure 6, where it is seen that our method achieves visually pleasing results by using only one epoch of fine-tuning. This shows that our model can adapt to new data very quickly demonstrating very good generalization capability. Training one epoch of the VOTES model takes 90 seconds on a machine with four GPUs.

5.4 Analysis of the VOTES Model

Shared video quality vs restoration performance As it is very clear that videos shared on social media will have lower quality than the source data, it will be interesting to see how the quality of the shared video affects restoration performance. To investigate this, we perform experiments on the validation set data in REDS. The videos are first down-scaled (by a factor of 2) and compressed with different quality parameters QP using the FFmpeg toolbox, then restored using various trained models in Section 5.2. Note that a smaller QP corresponds to a better quality or lower degradation. The performance curves are shown in Figure 8. It is seen that

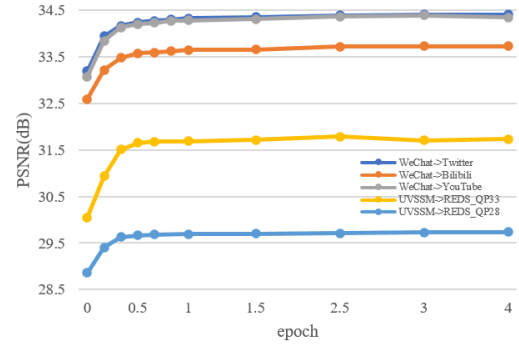


Figure 7: Cross-platform (from WeChat to Twitter, Bilibili and Youtube) and cross-dataset (from UVSSM to REDS) generalization.

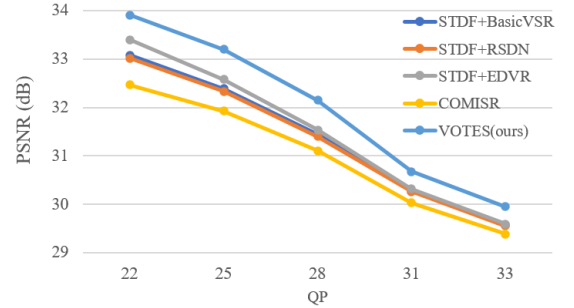


Figure 8: Restoration performance of different models for different quality (QP) videos. The results show here are averages of all testing videos in the REDS database.

our new model outperforms other models for every quality factor, demonstrating our model has good generalization capability across videos with different qualities.

How DFM relates to restoration errors An important innovative feature of the new VOTES technique is to adaptively estimate the DFM for each input frame, and use a CNN module to extract hierarchical features from the DFM to modulate the end-to-end video restoration neural network. We reason that the DFM contains important information indicating where in a frame it is more difficult to restore and that, through the framework in Figure 1, we will

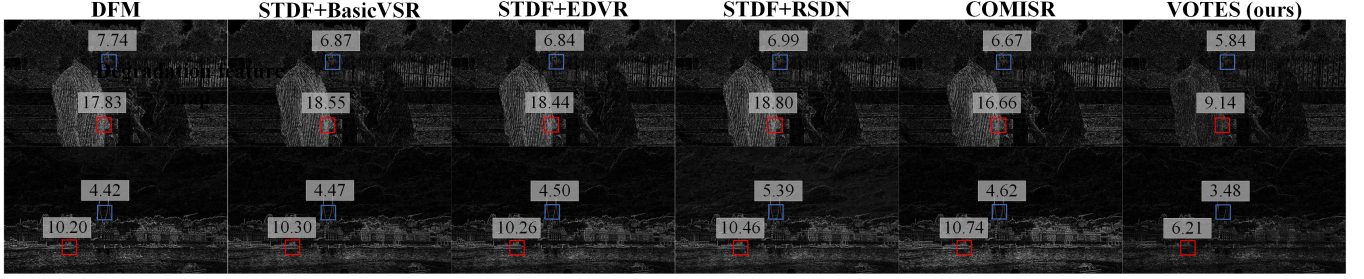


Figure 9: Relation between the DFM and restoration error. The examples are from UVSSM. The DFMs are in the 1st column, the rest are actual restoration errors of different methods. The number above each red box is the average element value within the red box. Note the original resolution of the DFM is half of that of the actual restoration error image, it is resized here for visualisation convenience.

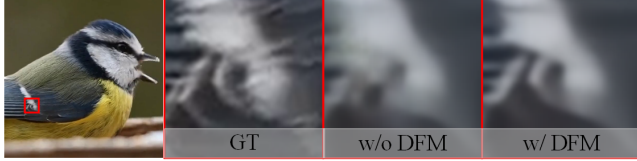


Figure 10: Visual comparison of restoration results with and without including the DFM, the w/o DFM image is more blurry than the w/ DFM image.

Table 3: Ablation study on the effectiveness of the DFM. "w/o" represents "without" and "w" represents "with". Blod text indicates the best.

| datasets | scale | QP | w/o DFM | w/ DFM |
|----------|------------|----|--------------|---------------------|
| REDS | $\times 2$ | 28 | 31.11/0.8465 | 32.15/0.8644 |
| | | 33 | 29.39/0.7912 | 29.95/0.8043 |
| | $\times 4$ | 28 | 27.10/0.7170 | 27.98/0.7410 |
| | | 33 | 26.08/0.6777 | 26.56/0.6926 |
| UVSSM | $\times 2$ | - | 31.35/0.8755 | 33.01/0.8945 |

be better able to extract features to restore those difficult regions. Figure 9 shows examples of DFMs and their corresponding final restoration error images by five different methods. It is clearly seen that if an area in the DFM has a larger value, then the corresponding area in the final restored images of all the methods will have a larger error, or vice versa. This clearly demonstrates the correctness of our reasoning that the DFM can indicate where it is more difficult to restore. Importantly, it is also seen that our model always achieves the lowest errors across all areas of the image, demonstrating that we have achieved our design objective and that the estimated DFM has indeed helped improve the performance of the end-to-end video restoration network. More visual examples of how DFM relates to restoration errors are included in supplementary material.

The effectiveness of the DFM To analyse the effectiveness of the degradation feature map, we conduct an ablation study. We set $DFM = 0$ (all elements in DFM are set to zero) to represent the case when DFM is not included in the framework. Figure 10 shows a visual example where it is seen that results without the DFM

Table 4: Performance of models with different n .

| n | 7 | 8 | 9 | 10 | 11 | 12 |
|------|-------|-------|-------|-------|-------|-------|
| PSNR | 33.71 | 33.64 | 33.86 | 33.89 | 33.88 | 33.86 |

have more pronounced motion-blur artifacts than that with DFM. The quantitative results in Table 3 also show the effectiveness of including the DFM. In general, the inclusion of the DFM produces better visual quality and improves quantitative performance.

Design of the degradation modulation module The estimated DFM is fed to a series of convolutional blocks to extract hierarchical degradation features which are then used to modulate the feature maps in the end-to-end restoration network. Table 4 shows the PSNR performance when a different number of convolutional blocks n was used to restore the videos shared on WeChat. It is seen that $n > 9$ gives stable performance, we therefore empirically use 10 convolutional blocks in the experiments.

6 CONCLUDING REMARKS

In this paper, we have developed a general video restoration method and applied it to the problem of restoring user videos shared on social media. A characteristic of such videos is that the types of degradation the videos have undergone are unknown. To address such problems we have developed the video restoration through adaptive degradation sensing (VOTES) framework, in which we first introduced the degradation feature map (DFM) concept to measure the difficulty of restoring each location of a frame and then, used convolutional operations to extract hierarchical degradation features from the DFM to modulate an end-to-end video restoration backbone neural network such that more attention can be paid to the more heavily degraded areas, which in turn helped improving the restoration results both visually and quantitatively. We have also contributed a large database for researching the problem of restoring user videos shared on social media platforms.

ACKNOWLEDGMENTS

This work was supported by the Guangdong Basic and Applied Basic Research Foundation (No. 2021A1515011584), Guangdong Basic and Applied Basic Research Foundation (Grant 2019B151502001) and Shenzhen R&D Program (Grant JCYJ20200109105008228).

REFERENCES

- [1] Kelvin C.K. Chan, Xintao Wang, Ke Yu, Chao Dong, and Chen Change Loy. 2021. BasicVSR: The Search for Essential Components in Video Super-Resolution and Beyond. In *2021 IEEE/CVF Conference on Computer Vision and Pattern Recognition (CVPR)*. 4945–4954.
- [2] Honggang Chen, Xiaohai He, Chao Ren, Linbo Qing, and Qizhi Teng. 2018. CISRDNN: Super-resolution of Compressed Images Using Deep Convolutional Neural Networks. *Neurocomputing* 285 (2018), 204–219.
- [3] Tao Dai, Jianrui Cai, Yongbing Zhang, Shu-Tao Xia, and Lei Zhang. 2019. Second-order Attention Network for Single Image Super-Resolution. In *2019 IEEE Conference on Computer Vision and Pattern Recognition (CVPR)*. 11065–11074.
- [4] Jianing Deng, Li Wang, Shiliang Pu, and Cheng Zhuo. 2020. Spatio-Temporal Deformable Convolution for Compressed Video Quality Enhancement. In *Proceedings of the Conference on Artificial Intelligence*, Vol. 34. 10696–10703.
- [5] Xueyang Fu, Zheng-Jun Zha, Feng Wu, Xinghao Ding, and John Paisley. 2019. JPEG Artifacts Reduction via Deep Convolutional Sparse Coding. In *2019 IEEE/CVF International Conference on Computer Vision (ICCV)*. 2501–2510.
- [6] Jinjin Gu, Hannan Lu, Wangmeng Zuo, and Chao Dong. 2019. Blind Super-Resolution With Iterative Kernel Correction. In *2019 IEEE/CVF Conference on Computer Vision and Pattern Recognition (CVPR)*. 1604–1613.
- [7] Zhenyu Guan, Qunliang Xing, Mai Xu, Ren Yang, Tie Liu, and Zulin Wang. 2021. MFQE 2.0: A New Approach for Multi-Frame Quality Enhancement on Compressed Video. *IEEE Transactions on Pattern Analysis and Machine Intelligence* 43, 3 (2021), 949–963.
- [8] Takashi Isobe, Xu Jia, Shuhang Gu, Songjiang Li, Shengjin Wang, and Qi Tian. 2020. Video Super-resolution with Recurrent Structure-detail Network. In *European Conference on Computer Vision*. Springer, 645–660.
- [9] Takashi Isobe, Songjiang Li, Xu Jia, Shanxin Yuan, Gregory Slabaugh, Chunjing Xu, Ya-Li Li, Shengjin Wang, and Qi Tian. 2020. Video Super-Resolution With Temporal Group Attention. In *2020 IEEE/CVF Conference on Computer Vision and Pattern Recognition (CVPR)*. 8005–8014.
- [10] Jiwon Kim, Jung Kwon Lee, and Kyoung Mu Lee. 2016. Accurate Image Super-Resolution Using Very Deep Convolutional Networks. In *2016 IEEE Conference on Computer Vision and Pattern Recognition (CVPR)*. 1646–1654.
- [11] Diederik P. Kingma and Jimmy Ba. 2015. Adam: A Method for Stochastic Optimization. In *2015 International Conference on Learning Representations (ICLR)*, Yoshua Bengio and Yann LeCun (Eds.).
- [12] Wei-Sheng Lai, Jia-Bin Huang, Narendra Ahuja, and Ming-Hsuan Yang. 2017. Deep Laplacian Pyramid Networks for Fast and Accurate Super-Resolution. In *2017 IEEE Conference on Computer Vision and Pattern Recognition (CVPR)*. 5835–5843.
- [13] Yinxiao Li, Pengchong Jin, Feng Yang, Ce Liu, Ming-Hsuan Yang, and Peyman Milanfar. 2021. COMISR: Compression-Informed Video Super-Resolution. In *2021 IEEE/CVF International Conference on Computer Vision (ICCV)*. 2523–2532.
- [14] Bee Lim, Sanghyun Son, Heewon Kim, Seungjun Nah, and Kyoung Mu Lee. 2017. Enhanced Deep Residual Networks for Single Image Super-Resolution. In *2017 IEEE Conference on Computer Vision and Pattern Recognition Workshops (CVPRW)*. 1132–1140.
- [15] Yiqun Mei, Yuchen Fan, and Yuqian Zhou. 2021. Image Super-Resolution With Non-Local Sparse Attention. In *Proceedings of the IEEE/CVF Conference on Computer Vision and Pattern Recognition (CVPR)*. 3517–3526.
- [16] Seungjun Nah, Sungyong Baik, Seokil Hong, Gyeongsik Moon, Sanghyun Son, Radu Timofte, and Kyoung Mu Lee. 2019. NTIRE 2019 Challenge on Video Deblurring and Super-Resolution: Dataset and Study. In *2019 IEEE/CVF Conference on Computer Vision and Pattern Recognition Workshops (CVPRW)*. 1996–2005.
- [17] Mehdi S. M. Sajjadi, Raviteja Vemulapalli, and Matthew Brown. 2018. Frame-Recurrent Video Super-Resolution. In *2018 IEEE Conference on Computer Vision and Pattern Recognition (CVPR)*.
- [18] Wang Shen, Wenbo Bao, Guangtao Zhai, Li Chen, Xiongkuo Min, and Zhiyong Gao. 2020. Blurry Video Frame Interpolation. In *2020 IEEE/CVF Conference on Computer Vision and Pattern Recognition (CVPR)*. 5113–5122.
- [19] Wenzhe Shi, Jose Caballero, Ferenc Huszar, Johannes Totz, Andrew P. Aitken, Rob Bishop, Daniel Rueckert, and Zehan Wang. 2016. Real-Time Single Image and Video Super-Resolution Using an Efficient Sub-Pixel Convolutional Neural Network. In *2016 IEEE Conference on Computer Vision and Pattern Recognition (CVPR)*. 1874–1883.
- [20] A. Murat Tekalp, Michele Covell, Radu Timofte, and Chao Dong. 2021. Editorial: Introduction to the Issue on Deep Learning for Image/Video Restoration and Compression. *IEEE Journal of Selected Topics in Signal Processing* 15, 2 (2021), 157–161.
- [21] Yapeng Tian, Yulun Zhang, Yun Fu, and Chenliang Xu. 2020. TDAN: Temporally-Deformable Alignment Network for Video Super-Resolution. In *2020 IEEE/CVF Conference on Computer Vision and Pattern Recognition (CVPR)*. 3357–3366.
- [22] Suramya Tomar. 2006. Converting video formats with FFmpeg. *Linux Journal* 2006, 146 (2006), 10.
- [23] Longguang Wang, Yingqian Wang, Xiaoyu Dong, Qingyu Xu, Jungang Yang, Wei An, and Yulan Guo. 2021. Unsupervised Degradation Representation Learning for Blind Super-Resolution. In *2021 IEEE/CVF Conference on Computer Vision and Pattern Recognition (CVPR)*. 10576–10585.
- [24] Xintao Wang, Kelvin C.K. Chan, Ke Yu, Chao Dong, and Chen Change Loy. 2019. EDVR: Video Restoration With Enhanced Deformable Convolutional Networks. In *2019 IEEE/CVF Conference on Computer Vision and Pattern Recognition Workshops (CVPRW)*. 1954–1963.
- [25] T. Wiegand, G.J. Sullivan, G. Bjontegaard, and A. Luthra. 2003. Overview of the H.264/AVC video coding standard. *IEEE Transactions on Circuits and Systems for Video Technology* 13, 7 (2003), 560–576.
- [26] Kai Zhang, Luc Van Gool, and Radu Timofte. 2020. Deep Unfolding Network for Image Super-Resolution. In *2020 IEEE/CVF Conference on Computer Vision and Pattern Recognition (CVPR)*. 3214–3223.
- [27] Kai Zhang, Wangmeng Zuo, Yunjin Chen, Deyu Meng, and Lei Zhang. 2017. Beyond a Gaussian Denoiser: Residual Learning of Deep CNN for Image Denoising. *IEEE Transactions on Image Processing* 26, 7 (2017), 3142–3155.
- [28] Kai Zhang, Wangmeng Zuo, and Lei Zhang. 2018. Learning a Single Convolutional Super-Resolution Network for Multiple Degradations. In *2018 IEEE/CVF Conference on Computer Vision and Pattern Recognition (CVPR)*. 3262–3271.
- [29] Yulun Zhang, Kunpeng Li, Kai Li, Lichen Wang, Bineng Zhong, and Yun Fu. 2018. Image Super-resolution Using Very Deep Residual Channel Attention Networks. In *2018 European Conference on Computer Vision (ECCV)*. 286–301.
- [30] Yulun Zhang, Kunpeng Li, Kai Li, Bineng Zhong, and Yun Fu. 2019. Residual Non-local Attention Networks for Image Restoration. In *2019 International Conference on Learning Representations*.
- [31] Yulun Zhang, Yapeng Tian, Yu Kong, Bineng Zhong, and Yun Fu. 2018. Residual Dense Network for Image Super-Resolution. In *2018 IEEE/CVF Conference on Computer Vision and Pattern Recognition (CVPR)*. 2472–2481.
- [32] Xizhou Zhu, Han Hu, Stephen Lin, and Jifeng Dai. 2019. Deformable ConvNets V2: More Deformable, Better Results. In *2019 IEEE/CVF Conference on Computer Vision and Pattern Recognition (CVPR)*. 9300–9308.